# The Coupling Effects Between Floating Insulation Plates and the Thermal Convection in their Bottoms---- An Understanding of Continental Drift

Chenlin Fang, Siyuan Wang

Shenzhen College Of International Education, Guangdong, China

**Abstract.** The phenomenon of dumpling drift was discovered during a cooking process, which triggered our thinking of the continental drift. After refining the existing common problems, an experiment on the thermal convection interaction between the floating heat insulation plates and the bottoms is designed. Through controlling variables, this paper investigates the floating patterns of floating insulation plates of different sizes on a thermally convective surface and the principles behind them. The findings show that the appropriate sizing of a floating plate can result in the manifestation of cyclic reciprocating movement on the water's surface. The periodic movement observed in this phenomenon can be attributed to the obstruction of heat exchange between the water surface and the surrounding air by the floating plate. Consequently, alterations in the direction of water flow induce corresponding shifts in water temperature, which subsequently affect the movement direction of the floating plate. The final outcome is characterized by a periodic reciprocal movement of the floating plate as it interacts with the heat convection occurring at the bottom. Floating plates that are either undersized or oversized would remain stationary without exhibiting any cyclic drift. The decrease in water depth leads to a diminished thermal drive, thereby amplifying the cyclical nature of the motion shown by the floating plate. The above findings indicate that the dimensions of the continental plates present on the Earth's surface have an impact on both the velocity and duration of their movement. The observation that a plate that is too small stagnates on top of a subduction current, while a plate that is too large stagnates on top of an upwelling current, suggests that the smaller continent of New Zealand is likely to experience a decrease in elevation due to its location above a subduction current. Conversely, the larger continent of Africa is expected to undergo uplift and attain a higher elevation as a result of its position above an upwelling current.

**Keywords:** Floating insulation plates, thermal convection, continental drift.

## 1. Introduction

Thermal convection phenomena are prevalent in various natural systems. In the context of atmospheric circulation, the sun's heat energy induces the expansion of air at the Earth's surface, resulting in a decrease in density and subsequent upward movement. As the ascending air mass elevates, it undergoes a process of cooling, resulting in the dissipation of thermal energy into the higher layers of the atmosphere. The process of air cooling results in an increase in air density, which then leads to the downward movement of the air, so establishing an atmospheric convection cycle. An additional illustration may be seen in the context of ocean circulation, whereby the dissimilarity in solar radiation receipt between the equatorial region and the polar regions leads to the presence of warmer water near the equator in comparison to the poles. The circulation pattern of saltwater involves the transport of warm equatorial water towards the polar regions, where it undergoes cooling and densification. Subsequently, the denser water sinks to the seabed in the polar regions and finally reemerges to cycle back towards the equatorial regions.

In addition to its prevalence in the natural world, the phenomena of heat convection are also widely observed in our everyday lives. One prevalent illustration is the act of cooking and the process of boiling water. When a pot of cold water is heated, the water at the bottom of the pot undergoes expansion due to the input of heat. As a result, the density of this heated water decreases, causing it to rise to the surface and release heat into the surrounding air. Simultaneously, the cold water on the surface, having lost heat, experiences an increase in density and subsequently descends towards the bottom of the pot to be reheated. This process establishes a continuous cycle of heat convection within the pot.

Numerous natural phenomena, including the thermal convection observed in everyday situations, share a fundamental characteristic: the fluid experiences heating at its lower region and cooling at its upper region. The phenomenon of heat convection characterized by homogeneous heating at the bottom and cooling at the top is commonly referred to as Rayleigh-Bénard convection, which is a well-established classical model in academic literature. The model under review has undergone extensive study over the past century, as will be elaborated upon in Section 2.1. It has gained significant popularity in the examination of natural phenomena and the resolution of diverse technical challenges. Nevertheless, the model exhibits many drawbacks, one of which is its assumption of a high degree of homogeneity in both the upper and lower borders of the fluid. This assumption is often not met in numerous real-world scenarios. The uppermost layer of the Earth's mantle exhibits mantle convection and consists of continental and oceanic plates. It is noteworthy that the oceanic plate possesses a thermal conductivity approximately 100 times greater than that of the continental plate. Consequently, a significant portion of the heat is primarily dissipated through the oceanic plate, while the continental plate serves as a thermal insulator. The Rayleigh-Bénard convection model is rendered inapplicable in this scenario due to the presence of non-uniform upper boundary conditions.

The objective of this research is to address a thermal convection issue involving non-uniform upper boundary conditions. The issue arises from a phenomenon observed during the process of cooking dumplings. Upon being cooked, the dumplings typically rise to the water's surface. However, the cooked dumplings do not remain stationary on the surface, but rather are propelled by the flow of water, resulting in their continuous movement. Through prolonged observation, it has been noted that the movement of the dumplings exhibits a distinct periodic pattern of aggregation and dispersion. This problem involves the interaction between floating dumplings with heat insulation properties and open water, resulting in a non-uniform upper boundary condition. The presence of the dumplings affects the heat convection at the bottom, leading to a complex and unstable behavior. Consequently, the dumplings are subjected to drift, causing changes in the upper boundary condition. The interaction between the floating dumplings and the convection currents at the bottom gives rise to a complicated coupled system. An illustrative instance of a comparable interconnected system can be observed in the amalgamated configuration of the continental plate and mantle convection. The continental plate existed as a unified supercontinent approximately 300 million years ago, but has since fragmented, resulting in the dispersal of continents throughout the Earth's surface. Geologists predict that these continents will eventually converge again to form a new supercontinent in several hundred million years. In recent years, research findings have indicated that the adiabatic effect of continental plates on mantle convection may contribute to alterations in mantle convection, thereby influencing the movement of continental plates.

The aforementioned observation suggests the possibility of a shared underlying mechanism governing both dumpling drift and continental drift, which warrants further investigation for elucidation. In this study, we want to develop meticulous and manageable physical experiments to investigate the mechanism by which the motion of a floating adiabatic plate is coupled with thermal convection at its base. These experiments will offer valuable insights into the knowledge of continental plate motion, providing a basis for further experimental analysis.

## 2. Research progress at home and abroad

### 2.1 Rayleigh-Bénard convection

The initial stage in the investigation of the interaction between a floating adiabatic plate and thermal convection involves an examination of the concept of thermal convection. The prevailing standard model employed for the study of thermal convection is the Rayleigh-Bénard convection (RBD) model [1]. As depicted in Fig. 1, a cylindrical cavity is filled with a convecting liquid, such as water. The lower part of the cavity experiences uniform heating, while the upper part of the cavity undergoes uniform cooling. Following a period of concurrent heating at the lower part and cooling at the upper part, a significant circulation pattern emerges within the enclosed space, as depicted in Fig.

1. The underlying cause for the extensive circulation observed in this phenomenon can be attributed to the presence of a substantial volume of heated water at the lower depths. This heated water, driven by thermal expansion, rises upwards and naturally congregates to create a cluster of thermal plumes resembling mushrooms, which ascend directly towards the surface for cooling purposes. The cooled water at the uppermost part will undergo a spontaneous process of aggregation, resulting in the formation of a chilly plume that descends towards the lower part. This massive and extensive flow substantially enhances vertical heat transport.

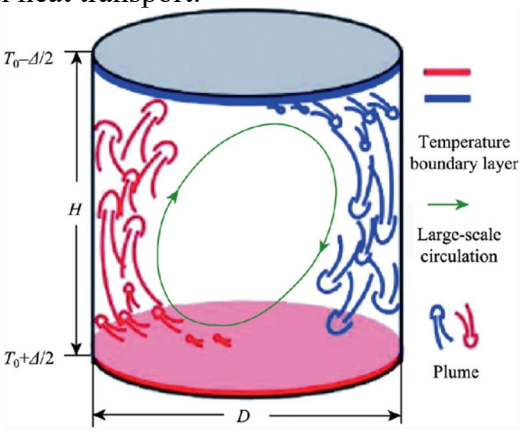

Figure 1. Rayleigh-Bénard convection (RBD) model

In this model, various physical properties of the fluid according to the Oberbeck-Boussinesq approximation, such as the coefficient of thermal expansion α (thermal expansion), the coefficient of Kinematic viscosity ν (Kinematic viscosity), the coefficient of thermal diffusivity κ (thermal diffusivity), etc., do not change with temperature. When buoyancy is considered, the density of the fluid $\rho$ is only linearly dependent on temperature $T$ linearly with temperature:

$$\frac{\rho}{\rho_0} = 1 - \alpha(T - T_0) \tag{1.1}$$

where $T_0$ is the average temperature of the fluid in the convection chamber, and $\rho_0$ is the average temperature of the fluid in the convection chamber, which is also the average density of the fluid. Under the Oberbeck-Boussinesq approximation, for an incompressible fluid, the governing equations of the system are as follows:

The continuity equation:

$$\nabla \cdot \vec{u} = 0 \tag{1.2}$$

Equation of motion of a fluid containing a buoyancy term (Navier-Stokes equation):

$$\frac{\partial \vec{u}}{\partial t} + \vec{u} \cdot \nabla \vec{u} = -\frac{1}{\rho}\nabla p + v\nabla^2 \vec{u} + \alpha g \delta T \vec{z} \tag{1.3}$$

Heat transport equation:

$$\frac{\partial \vec{T}}{\partial t} + \vec{u} \cdot \nabla T = \kappa \nabla^2 T \tag{1.4}$$

The above three equations together describe the velocity field in a convective cavity $\vec{u}(\vec{x}, t)$ and temperature field $T(\vec{x}, t)$ distribution in the convective cavity, where $\delta T = T - T_0$ is the position $\vec{x}$ of the fluid at the moment $t$ temperature of the fluid at the moment $T(\vec{x}, t)$ relative to the average temperature of the fluid in the convective cavity $T_0$ the amount of change in the temperature of the fluid in the convective cavity. It is noteworthy that the expression (1.3) corresponds to the well-known NS equation (Navier-Stokes equation) which incorporates a buoyancy term. The Navier-Stokes equation is a fundamental equation employed in the study of fluid dynamics, initially formulated by the renowned French engineer Navier and the Irish mathematician Stokes.

It is equivalent to Newton's second law of fluid motion, but since it is a highly complex nonlinear partial differential equation, no one has obtained its complete analytical solution so far. The generalized solution about the NS equation is even listed as one of the seven major mathematical problems of the world in the millennium [2]. It is for this reason that most of the current research in fluid mechanics is based on laboratory experiments and computer numerical simulations.

Equation (1.3) is the three-dimensional velocity vector $\vec{u}$ which is an expression for $\vec{u} = u\vec{x} + v\vec{y} + w\vec{z}$, where $\vec{x}$, $\vec{y}$, $\vec{z}$ correspond to the unit vectors in the three directions of the 3D coordinate axes x, y, and z, respectively, whereas u, v, w correspond to the projected components of the velocity vector in the three unit vector directions. Since the buoyancy force $\alpha g \delta T \vec{z}$ is acting in the vertical direction $\vec{z}$, we project equation (1.3) in the $\vec{z}$ direction projection is obtained as follows:

$$\frac{\partial w}{\partial t} + u\frac{\partial w}{\partial x} + v\frac{\partial w}{\partial y} + w\frac{\partial w}{\partial z} = -\frac{1}{\rho}\frac{\partial p}{\partial z} + v\frac{\partial^2 w}{\partial x \partial x} + v\frac{\partial^{2w}}{\partial y \partial y} + v\frac{\partial^2 w}{\partial z \partial z} + \alpha g \delta T \tag{1.5}$$

The heat transport equation (1.4) can be written as:

$$\frac{\partial \mathrm{T}}{\partial \mathrm{t}} + \mathrm{u}\frac{\partial \mathrm{T}}{\partial \mathrm{x}} + \mathrm{v}\frac{\partial \mathrm{T}}{\partial \mathrm{y}} + \mathrm{w}\frac{\partial \mathrm{T}}{\partial \mathrm{z}} = \kappa\frac{\partial^2 \mathrm{T}}{\partial \mathrm{x}\,\partial \mathrm{x}} + \kappa\frac{\partial^2 \mathrm{T}}{\partial \mathrm{y}\,\partial \mathrm{y}} + \kappa\frac{\partial^2 \mathrm{T}}{\partial \mathrm{z}\,\partial \mathrm{z}} \tag{1.6}$$

Furthermore, we will have the measured physical quantities in (1.5) and (1.6) $x, y, z, u, v, w, T, \delta T, t, p$ using the characteristic length H, characteristic velocity $u_{ff} = \sqrt{\alpha g H \Delta T}$. The characteristic temperature difference $\Delta T$is dimensionless to obtain a dimensionless physical quantity $\hat{x} = x/H$, $\hat{y} = y/H$,$\hat{z} = z/H$, $\hat{u} = u/\sqrt{\alpha g H \Delta T}$, $\hat{v} = v/\sqrt{\alpha g H \Delta T}$, $\hat{w} = w/\sqrt{\alpha g H \Delta T}$, $\hat{T} = T/\Delta T$,$\hat{t} = t/\left(H/\sqrt{\alpha g H \Delta T}\right)$,$\frac{\hat{p}}{\rho} = \frac{p}{\rho}/(\alpha g H \Delta T)$,Substituting these dimensionless physical quantities into (1.5) and (1.6) we obtain:

$$\frac{\partial \hat{w}}{\partial \hat{t}} + \frac{\partial \hat{w}}{\partial \hat{x}} + \hat{v}\frac{\partial \hat{w}}{\partial \hat{y}} + \hat{w}\frac{\partial \hat{w}}{\partial \hat{z}} = -\frac{1}{\hat{\rho}}\frac{\partial \hat{p}}{\partial \hat{z}} + \sqrt{\frac{Pr}{Ra}}\left(\frac{\partial^2 \hat{w}}{\partial x \partial x} + \frac{\partial^2 \hat{w}}{\partial y \partial y} + \frac{\partial^2 \hat{w}}{\partial z \partial z}\right) + \delta\hat{T} \tag{1.7}$$

$$\frac{\partial \hat{T}}{\partial \hat{t}} + \hat{u}\frac{\partial \hat{T}}{\partial \hat{x}} + \hat{v}\frac{\partial \hat{T}}{\partial \hat{y}} + \hat{w}\frac{\partial \hat{T}}{\partial \hat{z}} = \frac{1}{\sqrt{RaPr}}\left(\frac{\partial^2 \hat{T}}{\partial \hat{x}\partial \hat{x}} + \frac{\partial^2 \hat{T}}{\partial \hat{y}\partial \hat{y}} + \frac{\partial^2 \hat{T}}{\partial \hat{z}\partial \hat{z}}\right) \tag{1.8}$$

where (1.7) and (1.8) marked in blue determine the solution of the governing equations, i.e., the velocity and temperature field distributions. It can be seen that for a convective cavity of a given shape, the Rayleigh-Bénard convective system consists of only two dimensionless control parameters, the Rayleigh number $Ra = \alpha g \Delta T H^3/v\kappa$ and Prandtl number $Pr = v/\kappa$ for a given shape of convective cavity. $Ra$ is the dimensionless temperature difference representing the strength of the thermal drive (The greater the temperature difference$\Delta T$ between the upper and lower plates of the flow chamber, the greater the corresponding buoyancy, and the higher the $H$ height of the liquid, the buoyancy of the action of the longer distance, the two at the same time to react to the greater number of control parameter Ra). $Pr$ is the physical properties of the fluid parameters (reflecting the viscosity of the fluid and the relative strength of thermal diffusion; the greater the number of Pr the higher the viscosity of the fluid; for water, Pr is only related to the temperature, the higher the temperature the smaller the Pr).

With the control parameters Ra and Pr given, the state of the system is deterministic. For the state that should be determined, we usually use two response parameters Nusselt number $Nu = J_{Convection}/J_{conduction}$ and Reynolds number $Re = uL/v$ Nu to describe the system heat transfer efficiency and flow intensity. Nu denotes the dimensionless ratio between the heat $J_{Convection}$ actually transferred by convection in the system and the heat $J_{Convection} = X\Delta T/H$that could be transferred by the system in the absence of convection, relying solely on pure heat conduction. In this context, Nu is a function of the fluid's thermal conductivity. It is worth noting that a higher Nu value indicates a greater efficiency in the system's heat transport. It is commonly said in industrial settings that enhancing heat dissipation efficiency is tantamount to improving heat transport efficiency. Re is another dimensionless expression of the flow velocity u -- the larger Re represents the stronger the convective flow.

Previous studies of Rayleigh-Bénard convective systems have focused on the response parameters (e.g., the $Nu$ and $Re$) with the control parameters (e.g. $Ra$ and $Pr$). For example, the relationship between the response parameter Nu and the control parameter Ra is given in Fig. 2, where it can be seen that in a rather wide range (Ra from $10^6$ to $10^{17}$), Nu increases with the increase of Ra and presents the $Nu \propto Ra^{\beta}$ scalar rate relationship. More studies in this area can be found in [1].

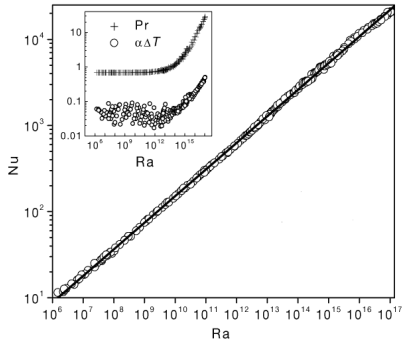


Figure 2 Plot of experimental relationship between $Nu$ and $Ra$ (from [3] Niemela et al, 2000)

## 2.2 Interaction of a floating adiabatic plate with thermal convection

The previous section focused on the characterization and conventional research methods of the Rayleigh-Bénard convection model, which is the standard model for thermal convection, but in fact the present study is much more complex compared to this standard model. As shown in Fig. 3, the Rayleigh-Bénard convection

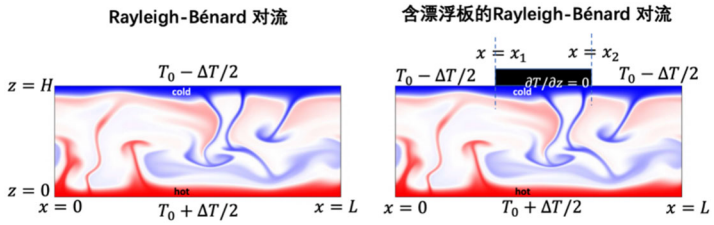


Figure 3. Rayleigh-Bénard convection and Rayleigh-Bénard convection with floating adiabatic plates

The boundary conditions of the flow model are fixed uniformly (upper boundary is uniformly cooled $T_{z=H} = T_0 - \Delta T/2$ and the lower boundary is uniformly heated$T_{z=0} = T_0 + \Delta T/2$ ). In this study, the lower boundary is fixed uniformly heated $T_{z=0} = T_0 + \Delta T/2$, but the upper boundary is composed of an adiabatic floating plate $\frac{\partial T_{z=H, x_1<x<x_2}}{\partial z} = 0$ and an open cooling region $T_{z=H, x<x_1 and\ x>x_2} = T_0 - \Delta T/2$ together. This means that the control parameters of the system will not only be $Ra$ and $Pr$, but also other control parameters such as the relative size of the floating plate $L_{□□□□□}/L_{cell}$ where $L_{□□□□□}$ is the length of the floating plate, and $L_{□□□□}$ is the total length of the vessel. The selection of this parameter is described in detail in Section 5.

As depicted in Fig. 3, the heat insulating plate, when situated on the upper surface of the heat convection, obstructs a portion of the liquid from coming into contact with the surrounding air. Consequently, this impedes effective cooling of the obstructed liquid, leading to a modification in the shape of the heat convection. Conversely, the underside of the buoyant plate exhibits flow in all directions, which imparts a net force on the plate, resulting in its displacement along a specific trajectory. When the plate is displaced, the liquid surface that was previously obstructed is once again exposed to contact with air. This results in the re-cooling of the liquid at that specific spot, therefore altering the flow dynamics. The aforementioned scenario illustrates the interaction between the floating adiabatic plate and thermal convection, resulting in a highly intricate problem. The forthcoming presentation will provide an update on the advancements made in the investigation of this issue.

In 1966, Wilson proposed the renowned Wilson cycle idea, which posits that the Atlantic Ocean undergoes a recurring sequence of closure and reopening over a span of around 300-500 million years [4]. In 1964, Bott and in 1967, Elder proposed the concept that the movement of continental plates is driven by convection currents in the mantle [5,6]. In a study conducted by Gurnis in 1988 and Whitehead in 2015, it was shown that the continental plate exerts an influence on the underlying thermal convection. This influence, in turn, induces movement in the continental plate. The observed phenomenon exhibits a distinct periodic pattern (Gurnis & Whitehead, 2015; Gurnis, 1988). The year

2000. The phenomenon of periodic drift shown by the insulating plate was seen for the inaugural time during a controlled laboratory experiment. The experimental results indicated that when the insulating plate is immobilized, a thermal plume emerges at its base. Conversely, upon releasing the plate, the thermal plume propels the plate to undergo drift [9]. In recent years, Mao conducted computer-based 2D numerical simulations to investigate the occurrence of cyclic drift behavior in thermal insulation plates. The findings indicate that not all plates exhibit this behavior. The occurrence of cyclic drift is found to be dependent on the size of the plates, with smaller plates tending to stagnate and oscillate at a fixed position. When the ratio of the plate length to the length of the convection groove reached around 1/4, the plate exhibited periodic reciprocal motion. As the plate length increased to 1/2 of the convection groove length, the plate displayed periodic motion. Furthermore, it was observed that larger plates had shorter motion periods [10, 11]. In conclusion, it is evident that there is currently a lack of empirical research establishing a direct correlation between plate size and the plate drift law. Consequently, our research project aims to investigate the drift law of floating plates of varying sizes within a consistent thermal convection system. Subsequently, we will analyze the underlying principles governing the interaction between plates of different sizes and thermal convection.

## 3. Introduction to the experimental setup

The proposed experiment entailed the placement of floats of varying sizes, such as bowls, into a pot of boiling water, with the objective of examining the resulting movement patterns. However, there are two inherent issues associated with this experimental design. One primary issue arises from the inherent inability to concurrently monitor and analyze the movement patterns within the aquatic environment. Consequently, our understanding is limited to solely discerning the movement patterns of the floats, while failing to elucidate the mechanisms by which the water flow propels these floats. The outcome of this phenomenon is that our knowledge is limited to what we are aware of, while our lack of knowledge remains unknown to us. The second issue is to the complexity of measuring the law of motion for the float in the pot due to its two-dimensional horizontal motion, which is considerably more intricate than motion confined to a single dimension. The experimental setup depicted in Fig. 4 was constructed with the intention of adhering to the idea of capturing the study's focus and streamlining the experimental design.

The experimental configuration consists of an acrylic convection tank with internal dimensions measuring 250 mm in length, 73.7 mm in width, and 125 mm in height. The selection of acrylic as the material of choice was based on its favorable thermal insulation properties and its ability to uniformly transmit light. The convection tank was filled with a homogeneous liquid, specifically pure water, at a vertical distance of 74.5 millimeters. In order to address the issue of gas bubbles present in the water, a method was employed wherein the water was subjected to boiling and subsequent cooling prior to each experimental trial. This process aimed to effectively remove the dissolved gases (degas) from the water. To induce thermal convection, a copper plate was positioned at the base of the convection tank, with a heating resistor wire inserted within the plate to facilitate even heating. Fig. 4 depicts the heated copper plate situated at the base of the convection tank, which serves the purpose of temperature measurement.

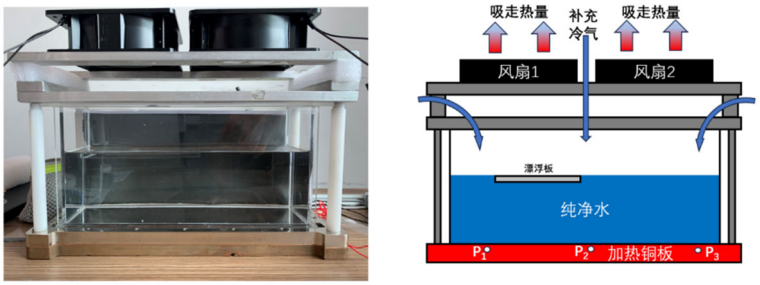

Figure 4. Real experimental setup (left) and experimental setup design (right)

Three holes were drilled at three different locations on the left, center and right, and three temperature probes $P_1$ , $P_2$ , $P_3$ were embedded (see Section 4 for the description of the temperature probes). The heat generated by the convection needs to be removed from the top, so we choose to install two fans to absorb the heat, and due to the continuity of the fluid, the corresponding cold air will also be drawn into the convection tank passively. The reason for choosing fans to absorb heat instead of the more efficient direct cold air blowing on the fluid surface is to minimize the effect of air flow on the motion of the floating plate.

Selecting the appropriate floating plate proved to be the most challenging aspect of this experiment. Attempts were made to utilize wooden plates and foam plates in the convection tank, but these materials proved ineffective as they exhibited a tendency to adhere to the sidewalls of the tank due to the surface tension of the water, hence impeding their ability to float unrestrictedly. After doing extensive research and thorough investigation, we ultimately selected the acrylic plate as the optimal choice for the floating plate due to its density closely resembling that of water. Fig. 5 illustrates the phenomenon of an acrylic plate floating in water when observed from the side view of the convection chamber. This floating is attributed to the influence of water surface tension, which causes the formation of a curved liquid surface along the edges of the plate. Despite the acrylic material having a slightly higher density than water, it still manages to float on the water's surface. Additionally, the curved liquid surface on both sides of the acrylic plate prevents its adhesion to the front and back walls of the convection groove. Naturally, this procedure necessitates a meticulous approach, wherein the acrylic plate must be gradually and horizontally positioned into the water surface. Any slight application of uneven force during this process may result in the acrylic plate tilting and subsequently sinking to the bottom of the water.

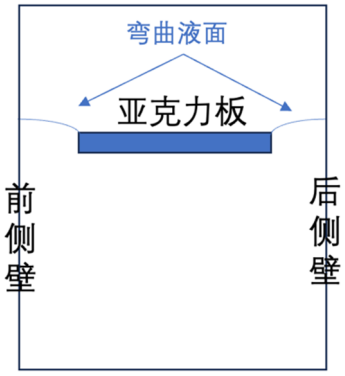


Figure 5. Side view of convection chamber containing a floating plate on the water surface

## 4. Introduction to experimental measurement tools

There are three primary measurement needs for this experiment, the first being temperature measurement, the second being velocity measurement, and the third being image grabbing of the floating plate position. Each of these three means of measurement and analysis will be described in the following three sections.

### 4.1 Temperature measurement

In order to achieve sensitive temperature measurements, two types of probes for temperature measurement were chosen, a large temperature probe with a probe size of 2.5 mm (OMEGA Engineering, Model 44031) and a small temperature probe with a probe size of 0.3 mm (Measurement Specialities Model: G22K7MCD419), as shown in Fig. 6.. The large temperature probe was used to measure the temperatures of $P_1$ , $P_2$ , $P_3$ in the heated copper plate shown in Fig. 4. Since the large temperature probe could not soak in water, the temperatures inside the experimental convection pure water were measured by the small temperature probe.

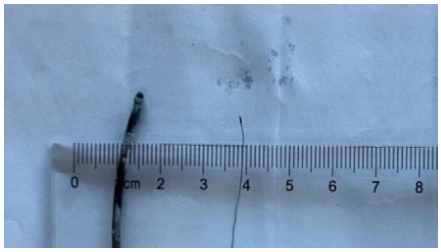

Figure 6. Large and small temperature probes

Both of these temperature probes are thermistors, and the principle of temperature measurement is the application of the Sternhar-Hart equation

$$\frac{1}{T} = a_1 ln^3 R + a_2 ln^2 R + a_3 lnR + a_4$$

The directly measured resistance R is converted to the desired temperature T. The parameters $a_1$ , $a_2$ , $a_3$ , $a_4$ in the formula are different for each temperature probe and need to be obtained in advance by temperature calibration (the calibration process is not described here).

### 4.2 Velocity measurement

After literature research, the commonly used velocity measurement in the field of fluid dynamics is the laser Particle Image Velocimetry, and the complete laser particle velocity measurement system is expensive (nearly half a million dollars) and complicated to build. In this project, we choose a simplified version of the laser particle velocity measurement method as shown in Fig. 7. First, a certain amount of 50μm particles with a density of 1.03g/cm$^3$ was poured into a convection tank, and the laser was turned on after the particles had been uniformly distributed in the tank.

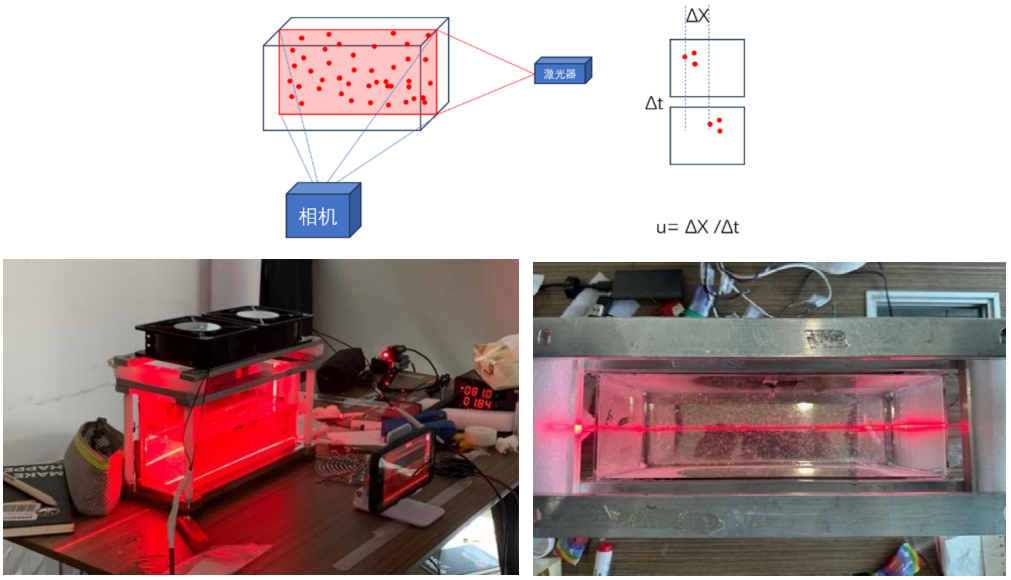


Figure 7. Principle of the laser particle velocity measurement method (top) and physical drawing (bottom).

A 500 mW continuous laser will illuminate a specific viewing plane in the fluid shown in Fig. 7. At the same time, the camera will take two consecutive pictures at a specific time interval $\Delta t$. Since the particles in the observation plane move along with the fluid, the velocity of the particles can be further calculated by comparing the particle positions in the two pictures to calculate the displacement $\Delta X$, which can be further calculated by $v = \Delta X/\Delta t$. Since the particles move with the fluid, the velocity of the fluid at that position is equivalent to the velocity of the nearby particles. The above is a brief introduction to the principle of laser particle velocity measurement, the actual operation will not track each particle, but will first be photographed to split the photo into a grid, there will be a certain number of particles in each grid, the $\Delta t$ shot of the two images of the grid particles for the calculation of the correlation between the grid particles in $\Delta t$ time can be obtained from the grid particles in $\Delta t$ time the average displacement of particles in order to get the average speed of the

particles in the grid. average velocity of the particles in the grid. The velocity field is obtained by combining all the flow velocities in the grid.

### 4.3 Measurement of the trajectory of a floating plate

The project has a challenging issue in determining the pixel position of the floating plate from the collected image. After multiple iterations, the technique for capturing images, as depicted in Fig. 8, was successfully identified.

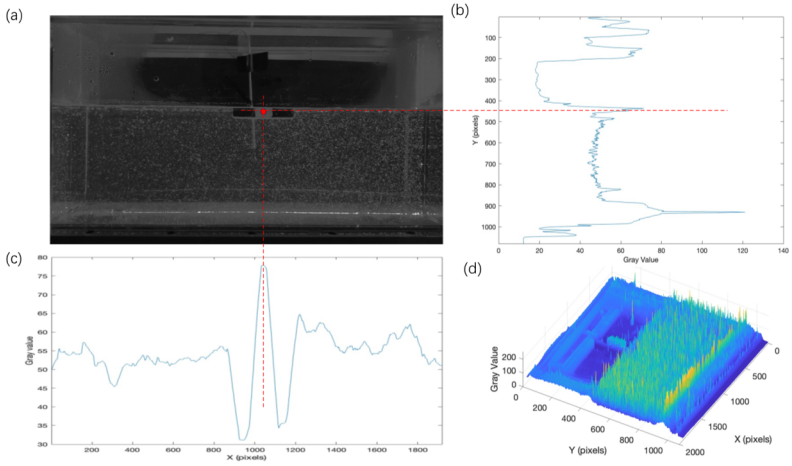


Figure 8. Method of grabbing the position of the floating plate in the image

It is well known that every electronic picture is composed of many smallest pixel units, take the 1080*1920 pixel Fig. 8a for example, our goal is to identify the position coordinates of the center of the floating plate in this Fig. 8 by a computer program. First, the image in Fig. 8a is imported into Matlab to obtain a 1080*1920 grayscale matrix, and each element in the matrix corresponds to the grayscale value of that position (black corresponds to a grayscale value of 0, and white corresponds to a maximum grayscale value of 255). This grayscale matrix is drawn in a 3D coordinate system as shown in Fig. 8d. In the second step, this gray matrix is averaged along the horizontal direction to obtain Fig. 8b, where an algorithm (e.g., finding the local maximum of the Gray value) is applied to find the floating height of the floating plate Y = 450 pixel.In the third step, the gray matrix is averaged along the horizontal direction to obtain Fig. 8b, where an algorithm (e.g., finding the local maximum of the Gray value) is applied to find the floating height of the floating plate Y = 450 pixel. The gray matrix is averaged along the vertical direction to obtain Fig. 8c. The grayscale matrix is vertically superimposed and averaged to get Fig. 8c, where the position with the largest grayscale value is the center of the floating plate X=1040 pixel. Through the above three steps, we get the X=1040, Y=450 pixel position of the floating plate in the whole image. Finally, we convert the pixels into spatial dimensions proportionally to get the actual horizontal position and height of the floating plate.

## 5. Results

Four floating plates of different lengths were used in this experiment, numbered 1, 2, 3, and 4 from smallest to largest as shown in Fig. 9. They were 60.7 mm wide and 4.6 mm thick, with lengths of $L_1$ =39.7 mm, $L_2$ =60.5 mm, $L_3$ =121.4 mm, and $L_4$ =182 mm, which accounted for $L_1$ /L=0.16, L /L=0.24, L /L=0.48, and L /L=0.73, respectively, of the length of a container with a total length of L=250 mm. $L_2$ /L=0.24, $L_3$ /L=0.48, and $L_4$ /L=0.73, respectively. In the following part, we use $\frac{L_{□□□□}}{L_{cell}}$ to represent the size of the floating plate relative to the length of the container.

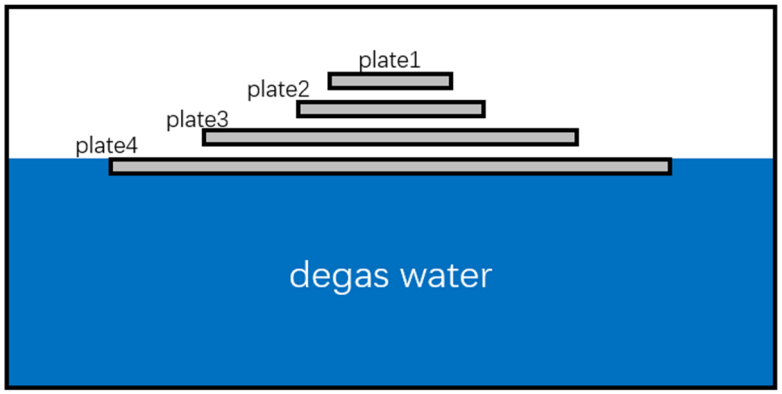


Figure 9. Schematic diagram of four different sizes of floating plates compared to the container size

In order to control the variables for easy comparison, we only changed the length of the floating plate in the four experiments, and all the rest of the experimental parameters were fixed. For example, the control parameters Ra=5e8, Pr=2.3 introduced in Section 2 were kept constant for the four experiments. In all experiments, the initial water level was set to 74.5mm, the heating power of the copper plate at the bottom was Pheating=$U^2$ /R=81*81/44=149W, and all experiments were completed in a constant temperature air-conditioned room at 21 degrees.

### 5.1 Summary of the floatation patterns of the four floating plates

In order to better characterize the position of the floating plates on the water surface, we define the center of the water surface as X = 0. Thus X > 0 means that the floating plates move to the right side. Fig. 10 shows the pattern of the left and right positions of the four floating plates over time. It should be noted that the vertical coordinates of all the plots show X/L instead of X, where L is the length of the entire container. X/L as a dimensionless physical quantity is a better visualization of the position of the plates than X. For example, when X/L = -0.25, we define the center of the water surface as X = 0, so that X > 0 means that the plate moves to the right side. For example, when X/L = -0.25, we know that the float has moved 1/4 container length left of center.

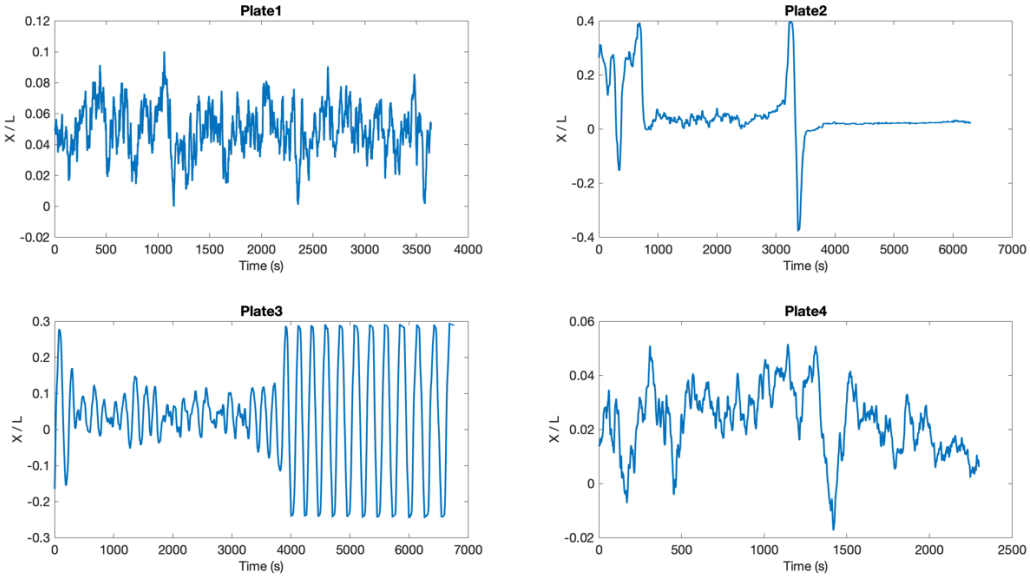


Figure 10. Plot of horizontal position X/L of four floating plates versus time (in seconds)

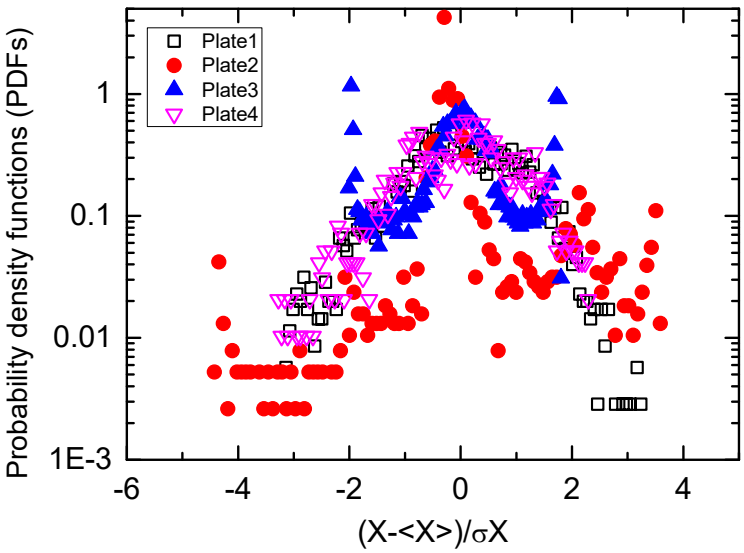


Figure 11. Probability density distribution of the horizontal position X/L of the four floating plates over the entire measurement time period

As can be seen in Fig. 10, the smallest Plate1 ($\frac{L}{L_{cell}} = 0.16$) and the largest Plate4 ($\frac{L}{L_{cell}} = 0.73$) are almost always stagnant with small oscillations around the center of the container. The larger size Plate2 ($\frac{L}{L_{cell}} = 0.24$) begins to show left-right motion across the entire length of the container, and the larger Plate3 ($\frac{L}{L_{cell}} = 0.48$) not only has left-right periodic motion across the entire length of the container, but also has a much shorter period of left-right reciprocal motion, with a measured reciprocal period of $\tau = 248$ s. Fig. 11 illustrates the probability density distributions of the horizontal positions of the four floating plates, and it can be seen that Plate1 and Plate4, which are represented by the hollow dots, show obvious single-peaked Gaussian distributions, which indicates that the corresponding plates mainly stay at their average positions at the main time neighborhood unchanged. Plate2 and Plate3 represented by solid dots, on the other hand, show more obvious multi-peak distributions, indicating that the corresponding plates do not stay at the average position most of the time but stay the longest on both sides of the average position, which also confirms the previous conclusion about the whole reciprocal motion.

It can be seen that it is not the case that the larger or smaller the size of the floating plate, the more frequently the floating plate will move back and forth periodically, but that there exists an appropriate size that makes the reciprocal motion the most frequent. This conclusion differs from the results obtained from Mao's computer numerical simulations in 2019, where Mao found that $\frac{L}{L_{cell}} > 0.25$ that the plates all have reciprocal drifts that span the entire length of the convection groove, which is in contrast to our finding of $\frac{L}{L_{cell}} = 0.73$ no reciprocal drift in the stagnant state [10]. This may be due to the fact that Mao's numerical simulation does not consider the mass of the floating plates but rather the mass of all the different sized plates is considered to be zero and the velocity of the floating plates is equal to the average flow velocity of the contacting water surface. In the experiment $\frac{L}{L_{cell}} = 0.73$, when the floating plate has a large mass, the bottom water current is no longer enough to drive it to a large extent.

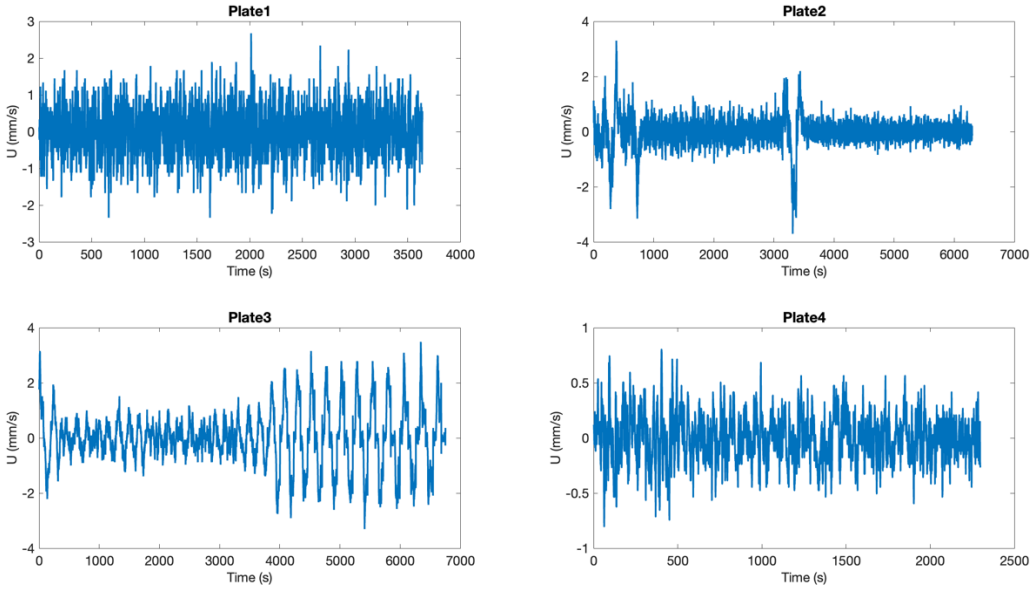


Figure 12. Plot of horizontal velocity (in mm/s) versus time (in s) for four floating plates

After obtaining the position of the floating plate at each moment, we further calculate to obtain the left and right drifting speed of the floating plate at each moment, as shown in Fig. 12. It can be seen that Plate4 has the slowest drifting speed, which is basically within 0.8 mm/s, Plate1's drifting speed mainly floats within 1 mm/s, and Plate2 and Plate3's drifting speeds exceed 2.5 mm/s when there is a clear periodic left-right reciprocating motion. It can be seen that the very large and very small floating plates do not have a periodic reciprocal motion across the entire size of the container, and so both have the smallest travel speed. The very large plate has a smaller acceleration for the same thrust because of its greater mass, so it moves at a smaller speed than the very small plate. The intermediate sizes that show significant periodic reciprocal motion$\frac{L}{L_{cell}} = 0.48$ The floating plate has the greatest speed of movement.

## 5.2 Velocity field analysis

After the introduction of the floating plate motion law in section 5.1, we want to delve into the underlying reasons for the occurrence of this particular motion law. The laser particle velocity measuring method described in section 4.2 is employed to observe the thermal convection flow at the lower surface of the plate under various plate motion conditions.

### 5.2.1 Thermal convection flow field corresponding to a stagnant floating plate

Since both Plate1 and Plate4 are almost stable in the center of the vessel without much displacement, the flow state of thermal convection at the bottom is relatively fixed. After nearly 1 hour of continuous shooting we obtained nearly 4000 velocity distribution fields respectively, and the results after averaging are shown in Fig. 13. The direction of the colored arrows in the Fig. 13 represents the average flow direction at the corresponding spatial location, and the length and color of the colored arrows both represent the average flow intensity. The black dashed arrows indicate the approximate flow direction of the fluid below the plate.

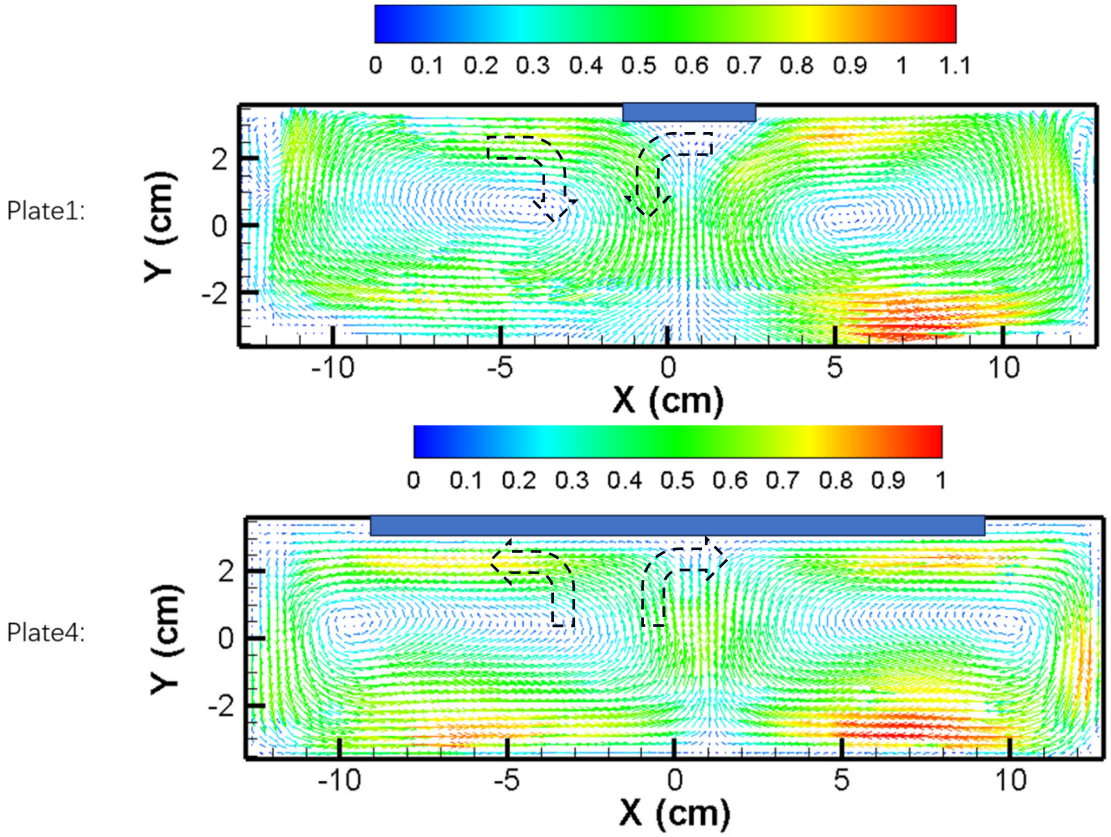


Figure 13. Bottom thermal convection flow field distribution corresponding to the smallest Plate1 and the largest Plate4 (velocity units cm/s)

As shown in Fig. 13, we find that for the smallest Plate1 ($\frac{L_{□□□□}}{L_{cell}} = 0.16$ ), it is in the middle of two circulations with opposite directions. The left side is a clockwise circulation and the right side is a counterclockwise circulation. The result is that the fluid on the left and right sides of the bottom of Plate1 flows towards the center of Plate1, and due to the viscous force of the fluid, two frictional thrusts pointing left and right towards the center are formed at the bottom of the plate, which balance each other and allow Plate1 to float stably in the center. At the bottom of Plate1 is an obvious subsidence flow. The conclusion is the same as the smallest plate introduced in Mao's article in 2019 $\frac{L_{□□□□}}{L_{cell}} = 0.03$ which has the same mechanism of motion. The difference is that Plate4 ($\frac{L_{□□□□}}{L_{cell}} = 0.73$ ) has a distinct upward flow at the bottom, which tops Plate4 and then flows separately toward the left and right sides, creating two tensile forces in opposite directions. These two pulls are equal in size allowing Plate4 to float steadily in the center. However Mao in his 2019 article notes that even the largest plates $\frac{L_{□□□□}}{L_{cell}} = 0.5$ also still observe significant reciprocal motion with shorter periods [10]. This difference may be due to the fact that Mao's computer numerical simulations do not take into account the inertial mass of the floating plate, which is a factor that cannot be ignored when the plate is very large. When the inertial mass is large, the viscous force from the bottom flow will be difficult to drive the plate movement.

In summary, it is concluded that although both the very small plate and the very large plate are stable in the center, the bottom of the former is a descending flow and the bottom of the latter is an ascending flow, and the former is stable because the left and right thrusts are balanced, while the latter is stable because the left and right pulls are balanced. The example of the subsidence flow at the bottom of the very small plate pulling down the height of the very small plate to some extent has its counterpart in geology. According to geological studies, 90% of New Zealand Island lies below the sea surface which is highly related to the convective subsidence flow of the mantle at its base [12]. On the contrary, the upwelling at the base of a very large plate can push up the plate's height to a

certain extent, and in geology, the southeastern part of the African continent has an average height of 1 km above sea level due to the strong upwelling of the bottom mantle convection [13].

**5.2.2 Thermal convective flow field corresponding to a floating plate in a moving state**

Plate2 and Plate3 have different thermal convective flow field structures at the bottom corresponding to different plate positions because of the obvious long-distance drift. Therefore, we select the flow field structures at different moments to show them separately.

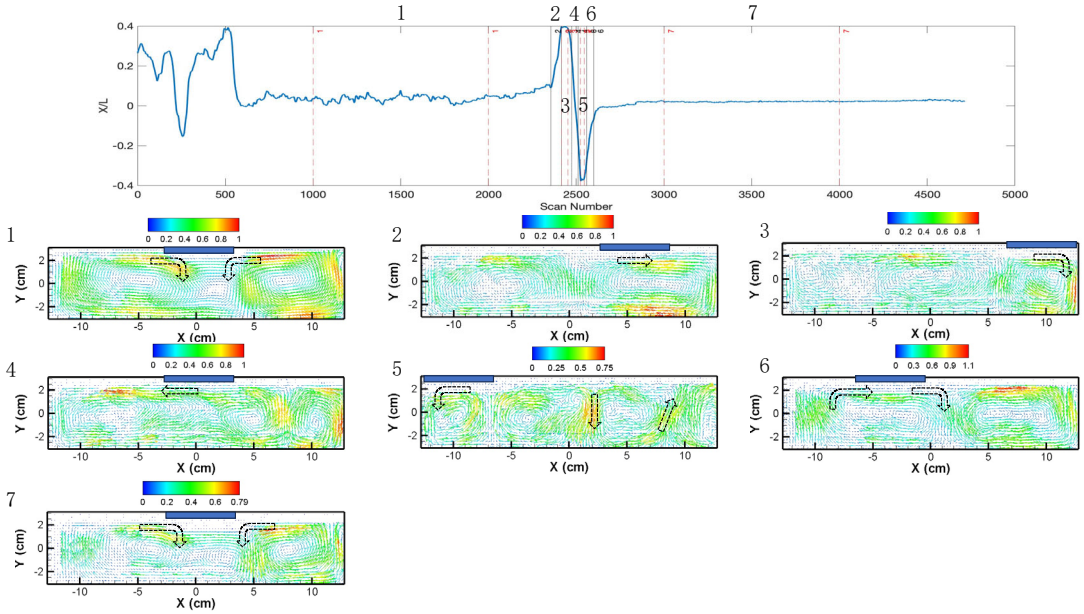


Figure 14. Plate 2 corresponds to the position of the plate and the average flow state (velocity in cm/s) for seven different time periods, from 1 to 7.

First we study the plate drift and the corresponding flow field structure of Plate2. As shown in Fig. 14, we can see that relative to the smallest Plate1, the somewhat larger Plate2 shows a clear left-right drift in the five time periods from 2nd to 6th. Seven velocity field distributions are obtained by splitting the whole shooting time into seven epochs. In the 1st and 7th time periods, the floating plate is basically immobile in the center, corresponding to the flow field analysis tells us that the bottom of the floating plate is flowing from the left and right sides to the center, which corresponds to the symmetric left and right thrusts that make the plate keep a fixed position during these time periods. However, this state of affairs does not last long, and in the second time period, the left side thrust is greater than the right side thrust causing the plate to leave the center position to reach the right side of the center position shown in Fig. 14-2. Because the plate insulation effect hinders the water and air contact at the corresponding position, resulting in a change in the flow direction of the water at that position, the water flow after the change in the flow direction will continue to drive the plate to the right until it reaches the right edge. Due to the container sidewall restrictions plate can not continue to the right and can only stay in place until the bottom of the flow direction is reversed again. After the reversal of the flow to drive the plate to the left to reach the position shown in Fig. 14-4, and then continue all the way to the left to reach the left edge of the container as shown in Fig. 14-5. Due to the restriction of the left wall of the container, the plate cannot continue to the left and has to stay in place until the flow direction at the bottom of the plate is reversed. The reversed flow drives the plate all the way to the right as shown in Fig. 14-6.

From the analysis of the above seven time periods, we can see that after the size of the plate becomes larger, its insulation effect begins to become obvious, obvious insulation effect makes the plate where the original bottom of the flow direction is reversed, the reversal of the flow direction so that the plate appears to have a certain period of reciprocating motion.

If we continue to increase the plate size to Plate3, we see a stronger periodic reciprocal motion of the plate.

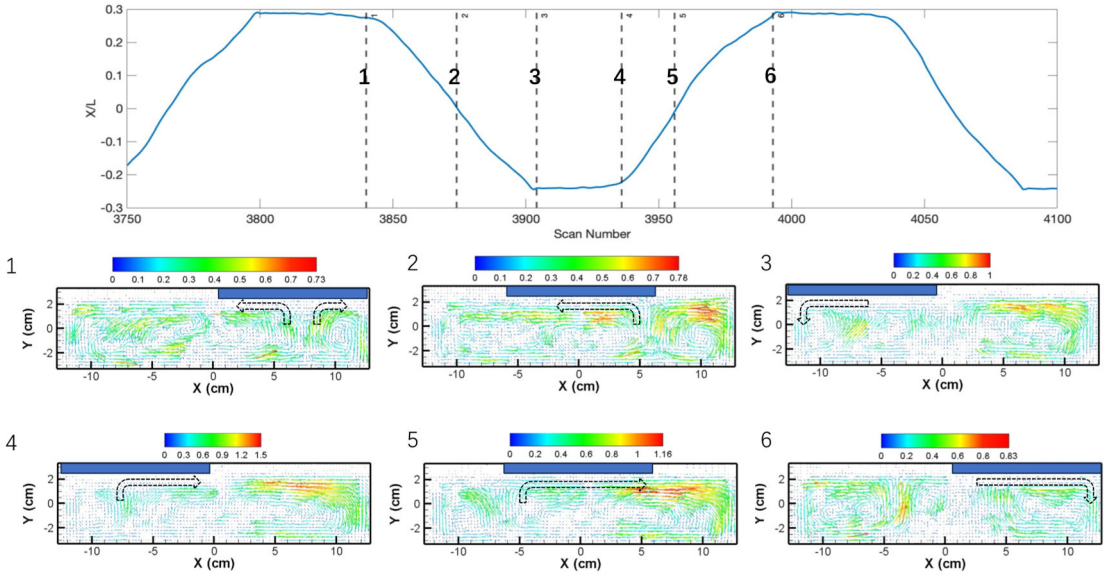


Figure 15. Plate2 plate position and average flow state (velocity in cm/s) corresponding to 7 different time periods from 1 to 7.

As shown in Fig. 15, near time period 1, the plate is about to start moving to the left, driven by the stronger flow to the left, the plate leaves the rightmost end to reach the center then continues to the left until it encounters a side wall and stops near time period 3. After stopping it waits until

At time period 4, the flow reversal at the bottom of the plate in turn drives the plate all the way to the right until time 6 reaches the far right end as shown in Fig. 15-6. Because Plate3 is larger than Plate2, it is better insulated, and the better insulation results in a shorter time for the flow reversal at the bottom of the plate, so the plate appears to move back and forth periodically more frequently. This explanation answers the question in section 5.1 as to why Plate3 was measured to reciprocate more frequently than Plate2.

### 5.3 Temperature distribution analysis

Using the temperature measurement method that was partially introduced in Section 4.1, we measured the temperatures corresponding to the left (P1), center (P2), and right (P3) positions of the bottom heating plate that were introduced in Fig. 4. Fig. 16 shows the temperatures of the heating plates in the four floating plate experiment

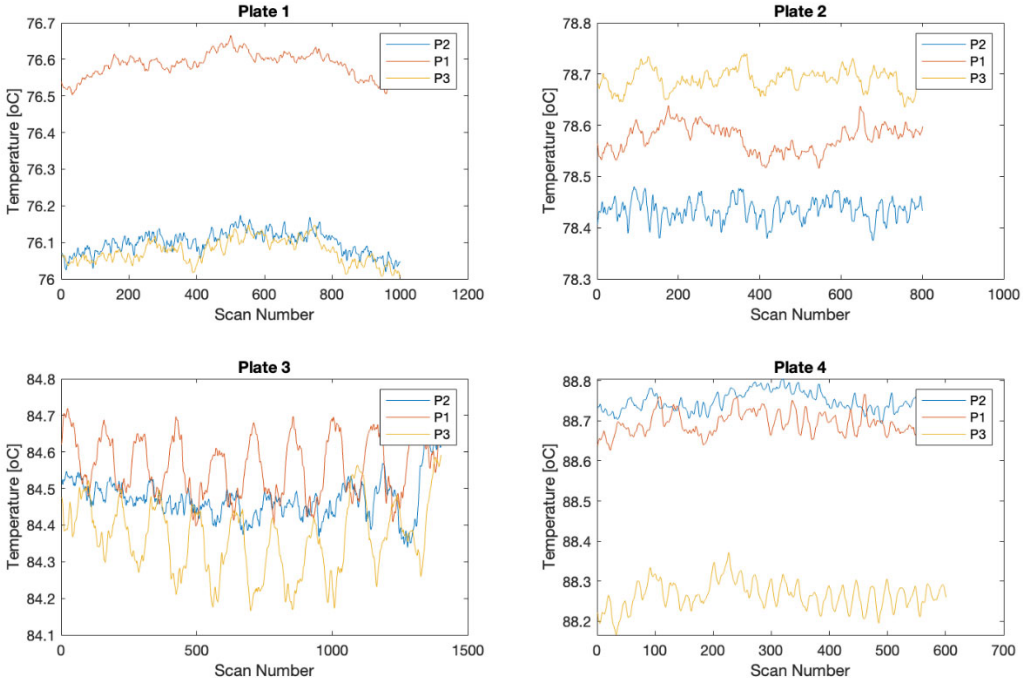


Figure 16. Temperatures corresponding to the left (P1), center (P2), and right (P3) positions of the bottom heating plate in the four floating plate experiment

changes, it can be seen that the temperature of the three positions of the heating plate are very close (maximum temperature difference of no more than 0.7 degrees Celsius), this is because of our experiments used to heat the copper plate thermal conductivity is very good, so that the heat distribution is very uniform. It is worth noting that Fig. 16, the lower left corner of the illustration shows the Plate3 experiments in the P1 (left) and P3 (right) position of the temperature change law over time, P1 and P3 temperature values show a completely opposite phase of the periodic law of change, which is precisely because the floating insulation plate in the left and right movement of the process of influencing the bottom of the heating plate temperature of the left and right position. When the heat insulation plate floats to the left, the temperature of the left side of the bottom heating plate will rise, when the heat insulation plate leaves the left side and floats to the right side, the temperature of the right side of the bottom heating plate will rise. This shows that the heat shield will change the direction of thermal convection by affecting the temperature of the fluid at the bottom of the shield.

It also enlightens us that because the thermal conductivity of the continental plate is about 1% of that of the oceanic plate, the insulating effect of the continental plate against mantle convection is very significant, and the temperature at the base of the continental plate rises no matter where it drifts to. When it rises to a critical point, mantle convection will push the continental plate to drift further.

## 6. Expanded Research (Change Ra)

In section 5, we got an important conclusion: whether the plate appears to have periodic reciprocal motion is related to the size of the plate, too small or too large plate will maintain a small oscillation at a fixed position, and only a specific size of the plate will have a frequent periodic large movement. In this experiment, when the size of the plate is the whole water surface area $\frac{L}{L_{cell}} = 0.48$ The periodic reciprocal motion was strongest when the plate was twice the size of the entire water surface. Returning to the introduction of the 4-plate experiment at the beginning of Section 5, we control the variables $Ra$=5e8, $Pr$=2.3, and vary the relative size of the floating plates$\frac{L}{L_{cell}}$ to investigate its effect on the experimental results. In this chapter we control $Pr$=2.3, *the* $\frac{L}{L_{cell}} = 0.48$ , varying

$Ra = \alpha g \Delta T H^3 / \nu K$ to study its effect on the experimental results. There are many ways to change the$Ra$ size can be done in many ways, two common practices one is to change the temperature difference between the top and bottom plates of the fluid by increasing the heating power $\Delta T$ and the other is to change the fluid height $H$ and the other is to change the height of the fluid. Since $Ra$ is proportional to the height $H$ is proportional to the third power, changing the $H$ to the height of the fluid has a greater effect on $Ra$ has a greater effect, so we decided to go with the second change in $H$

In the original four sets of experiments, the water depth was fixed at 74.5mm corresponding to $Ra = 5e8$. In this extension experiment, the water level was lowered to 40mm, which corresponded to a reduction of Ra by almost one order of magnitude to $Ra$=7e7, and then the floating period of Plate3 was investigated.

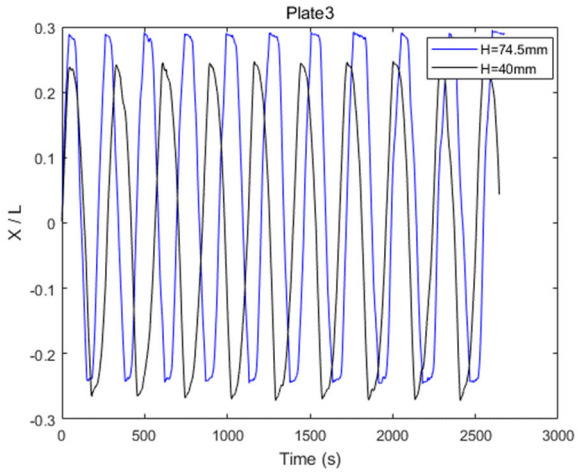


Figure 17. Horizontal position X/L of Plate3 (L3 /L=0.48) with time for water depths H=74.5mm ($Ra$=5e8) and H=40mm ($Ra$=7e7)

As shown in Fig. 17, we can see that the frequency of the reciprocating motion of the floating plate in the shallow water experiment (black line, H=40mm) is significantly slower than that of the reciprocating motion in the deep water experiment (blue line, H=74.5mm). After calculation, the period of the reciprocating motion of the floating plate in the shallow water experiment is $\tau_{H=40}$ = 278 s, and the period of the reciprocating motion of the floating plate in the deep water experiment is $\tau_{H=74.5}$ = 255 s. The period of the floating plate in the shallow water experiment increases by 9% compared with that in the deep water experiment, which is equivalent to a 9% slower frequency. To summarize, when the driving strength of thermal convection is reduced (by a factor of about 10 in Ra number), the flow slows down resulting in the period of the floating plate motion also slowing down by about 10%. This conclusion experimentally justifies the conclusion found by the computer simulations of Mao 2019 that decreasing the thermal driving strength Ra increases the plate drift period [10].

Extending this conclusion to geophysics we find that there is a relationship between the strength of mantle convection and the period of continental plate drift, suggesting that in the future we may be able to reverse engineer the strength of mantle convection through the period of continental plate drift, and hence the heat production power of the Earth's core.

## 7. Summary

Starting from the law found in daily life of cooking dumplings, this project has designed precise and controllable laboratory experiments through sufficient literature research. By comparing the effects of four groups of floating heat insulation plates with different sizes on the thermal convection, the following laws are summarized and the corresponding explanations are given:

A heat shield floating on the surface of the thermal convection will impede the contact of the liquid surface with the air and thus change the direction of the thermal convection flow.

Insulation plates with small sizes have a limited coverage area, resulting in a restricted impact on thermal convection. Consequently, they do not alter the direction of thermal convection. As a result, small insulation plates remain stationary at the center of the container, unaffected by the sinking flow location. The insulation plate with large sizes exhibits little movement, resulting in a challenge for the bottom flow to displace it. Consequently, the plate remains stationary at the center of the upward flow without undergoing any significant displacement.

Only moderately sized insulation plates (covering half of the water surface) will show a high frequency of reciprocal full motion.

Reducing the thermal drive strength Ra decreases the frequency of the reciprocating motion of the insulation plates.

This project proves the motion mechanism of Mao computer numerical about small and medium plates coupled with thermal convection from experimental point of view [10,11], and also points out that the mass of the floating plate is a non-negligible factor in the numerical simulation, because both the continental plate and the floating ice at sea in the real life have a large mass, which may bring incorrect conclusions if it is ignored. The results of this study reveal that the size of the continental plates on the Earth's surface is an important factor that affects the speed and period of their drift, and the strength of mantle convection also determines the period of continental plate drift. Finally, conclusion 2, "too small an insulating plate will stagnate above the subduction flow, and too large an insulating plate will stagnate above the upwelling flow", also has its role in geology. In geological explorations it has been found that 90% of the island of New Zealand lies below sea level [12] while the South African continent of East Africa is 1 km above sea level [13]. In conjunction with conclusion 2, we speculate that the reason for this may be that the smaller-sized New Zealand continent is dragged downward by stronger subsidence currents, while the larger-sized African continent is lifted up by stronger upwelling currents. Conclusion 4 helps us to establish a general relationship between the plate floatation period and the strength of thermal convection at the bottom, which, when quantified by more detailed studies in the future, will help us to infer the strength of mantle convection and the power of heat production in the Earth's inner core from the floatation period of the continental plates in reverse.

The duration of thermal convection experiments is significantly extended compared to conventional physics experiments, mostly due to the substantial time necessary to achieve a state of stable thermal convection. The experiment frequently encounters numerous challenges, including instances where the floating plates submerge or the apparatus experiences leakage over the course of the experiment. Consequently, the experiment generally necessitates repetition over an extended duration. In light of time and resource constraints, a selection was made to utilize solely four distinct floating plates of varying sizes for the sake of this experiment. In future investigations, it may be beneficial to incorporate more floating plates of varying sizes in order to conduct more comprehensive experiments that aim to quantify the correlation between the size of the floating plate and its duration of flotation. This approach would allow for a more complete exploration of the underlying physical factors that contribute to this relationship. Given that this experiment represents the inaugural investigation of thermal convection involving floating plates, a straightforward rectangular convection tank was selected as the experimental setup. The floating plates are capable solely of lateral movement within the confines of the convection tank, thereby enabling the concurrent measurement of the thermal convection velocity field through laser particle velocity measurement techniques. In future experiments, it is possible to implement a circular floating plate within a circular container, enabling controlled movement of the plate along a two-dimensional plane. This approach not only enhances the complexity of the experiment but also brings it closer to replicating the dynamics of the genuine continental drift model.

## Acknowledgements

First and foremost, we express our gratitude to our thesis adviser, who exemplifies qualities of seriousness, responsibility, and enthusiasm in their role as an educator. Throughout the process, he has provided us with substantial guidance and thorough revisions, imparting valuable knowledge. His stringent standards and rigorous approach serve as a paradigm for our future academic pursuits. We shall forever hold Mr. Jiang in our memory for his invaluable instruction, and we extend our utmost admiration and sincere gratitude to him. The knowledge imparted by our instructor has provided us with valuable insights that will have long-lasting advantages in our future endeavors.

Finally, we would like to express our gratitude to our family and close friends for their unwavering support throughout this duration. The affection and encouragement provided by our familial and social networks have served as the primary impetus for our continued perseverance. We express our heartfelt gratitude for the unwavering encouragement and support that they have always shown us, regardless of time or location.

## References

[1] Ahlers, G., Grossmann, S. & Lohse, D. 2009 Heat transfer and large scale dynamics in turbulent Rayleigh-Bénard convection. rev. mod. Phys. 81, 503-537.

[2] https://www.163.com/dy/article/EKCHUJ0K053299CD.html

[3] Niemela, J. J., Skrbek, L., Sreenivasan, K. R. & Donnelly, R. J. 2000 Turbulent convection at very high Rayleigh numbers. Nature 404, 837 -840.

[4] Wilson, J. T. 1966 Did the Atlantic close and then re-open? Nature 211 (5050), 676-681.

[5] Bott, M. H. P. 1964 Convection in the Earth's mantle and the mechanism of continental drift. Nature 259, 583-584.

[6] Elder, J. 1967 Convective self-propulsion of continents, Nature, 214(5089), 657-750, doi:10.1038/214657a0.

[7] Gurnis, M. 1988 Large-scale mantle convection and aggregation and dispersal of supercontinents. Nature 313, 541-546.

[8] Whitehead, J.A. & Behn, M.D. 2015 The continental drift convection cell. Geophys. Res. Lett. 42, 4301-4308.

[9] Zhang, J. & Libchaber, A. 2000 Periodic boundary motion in thermal turbulence. Phys. Rev. Lett. 84, 4361-4364

[10] Mao, Y., Zhong, J.-Q. & Zhang, J. 2019 The dynamics of an insulating plate over a thermally convecting fluid and its implication for continent movement over convective mantle. J. Fluid Mech. 868, 286-315.

[11] Mao, Y. 2021 An insulating plate drifting over a thermally convecting fluid: the effect of plate size on plate motion, coupling modes and flow structure. j Fluid Mech. 916, A18

[12] Suggate, R. P., Stevens, G. R. & Te Punga, M. T. 1978 The Geology of New Zealand. department of Scientific and Industrial Research.

[13] Lithgow-Bertelloni, C. & Silver, P. G. 1998 Dynamic topography, plate driving forces and the African superswell. nature 395, 269-272